Magnetic actuation of otoliths allows behavioral and brain-wide neuronal exploration of vestibulo-motor processing in larval zebrafish

Natalia Beiza-Canelo[1] **Hippolyte Moulle**[1] **Thomas Pujol**[1,2] **Thomas Panier**[1,3]

Geoffrey Migault[1] **Guillaume Le Goc**[1] **Pierre Tapie**[1] **Nicolas Desprat**[4] **Hans Straka**[5]

Georges Debrégeas[1]

Volker Bormuth[1,*]

[1] Sorbonne Université, CNRS, Institut de Biologie Paris-Seine (IBPS),
Laboratoire Jean Perrin (LJP), Paris, France.
[2] IBENS, Département de Biologie, Ecole Normale Supérieure, CNRS, Inserm,
PSL Research University, Paris, France.
[3] Sorbonne Université, CNRS, Institut de Biologie Paris-Seine (IBPS),
Plateforme d'Imagerie, Paris, France.
[4] Laboratoire de Physique de l'École normale supérieure, ENS,
Université PSL, CNRS, Sorbonne Université, Université Paris Cité, F-75005 Paris, France
Paris Diderot University, 10 rue Alice Domon et Leonie Duquet, 75013, Paris, France
[5] Faculty of Biology,
Ludwig-Maximilians-University Munich, Grosshadernerstr. 2, 82152 Planegg, Germany

[*] Corresponding : volker.bormuth@sorbonne-universite.fr

July 5, 2022

Abstract

The vestibular system in the inner ear plays a central role in sensorimotor control by informing the brain about the orientation and linear acceleration of the head. However, most neurophysiological experiments are performed using head-fixed configurations depriving animals of vestibular inputs. To overcome this limitation, we decorated the utricular otolith of the vestibular system with paramagnetic nanoparticles. This procedure effectively endowed the animal with magneto-sensitive capacities: applied magnetic field gradients induced forces on the otoliths resulting in robust behavioral responses comparable to that evoked by rotating the animal by up to 20°. We recorded the whole-brain neuronal response to this fictive vestibular stimulation using light-sheet functional imaging. Experiments performed in unilaterally injected fish revealed the activation of a commissural inhibition between the brain hemispheres. This magnetic-based stimulation technique opens new perspectives to functionally dissect the neural circuits underlying vestibular processing and to develop multisensory virtual environments including vestibular feedback.

***K*eywords** zebrafish · vestibular system · ferrofluid · magnetic actuation · zebrafish · whole-brain imaging · light-sheet microscopy

1 Introduction

The vestibular sense is crucial for evidence accumulation and decision making in every ethological behavior that involves body movements. The vestibular apparatus is located in the inner ear and comprises several organs that report on the various components of the acceleration forces. Rotational acceleration of the head induces an endolymph flow in the semicircular canals, which is detected by mechanosensitive structures called cupulae, respectively. Translational acceleration, as well as gravitational forces, act on two otolithic structures overlaying on the utricular and saccular epithelia, and whose motion is transduced by mechanosensitive hair cells to which they are coupled.

Neuronal signals encoding the head orientation and movement are relayed to neuronal circuits that drive compensatory movements in order to stabilize gaze and posture. Vestibular information is first processed in the brainstem vestibular nucleus and the cerebellum, which receive direct vestibular afferent input. Information is further distributed to oculomotor, skeletomotor, and autonomous motor systems, and in mammals, also via the thalamus to cortical systems [1]. At the various stages of signal processing, vestibular information is integrated with non-vestibular sources of self-motion information such as visual, somatosensory and proprioceptive inputs as well as locomotor efference copies [2].

In spite of the central role played by the vestibular system in sensorimotor tasks, most neuronal recordings are currently performed in animals deprived of any vestibular signals, i.e., under head- or body-fixed stationary conditions. This is due to the inherent challenge of combining neural recordings and natural vestibular stimulation as the latter necessitates to rotate or translate the animal's head in space, and is thus incompatible with head-fixed recording configurations required for most functional calcium imaging techniques.

Our knowledge on the vestibular system thus essentially derives from electrophysiological experiments in which the spike activity of a small number of neurons is sequentially monitored using implanted electrodes.

As vestibular processing is widely distributed across the brain, zebrafish constitutes a promising model animal to study the neuronal substrate of this highly conserved sensory system. The small size and transparency of the larval zebrafish brain indeed offers the unique opportunity to record cell-resolved brain-wide neuronal activity using light-sheet based calcium imaging [3, 4, 5, 6]. With the exception of the semicircular canals, which are still immature in young larvae [7], the vestibular system is mostly functional in larval zebrafish as early as 6 days post-fertilization [8], an age at which whole-brain imaging is routinely performed. This is evidenced by the capacity of the larvae to efficiently stabilize their posture and gaze in response to body rotation, via vestibulo-ocular and vestibulo-spinal reflexes [8, 4, 9, 10, 11].

Two experimental methods to provide controlled vestibular stimulation, while performing functional whole-brain imaging, were recently introduced. In the work from Migault *et al.* [4], we solved the problem by co-rotating the fish and the (miniaturized) light-sheet microscope, thus keeping the imaging volume unchanged during the stimulation. Favre-Bulle et al.[9, 5] generated a fictive vestibular stimulus using optical tweezers to displace the utricular otolith. Although these two approaches enable simultaneous neural recording, they both involve demanding optical developments that may hamper their broad diffusion among groups employing neurophysiological methods. Furthermore, the accessible stimulation range, in terms of maximal acceleration that they can emulate, is limited.

Here we present an alternative approach based on the magnetic actuation of the otoliths after surface coating by ferromagnetic nanoparticles. These superparamagnetic iron oxide nanoparticles are available in the form of colloïdal solutions called ferrofluids [12]. Although they do not carry a permanent magnetic moment, these particles acquire a magnetization in an externally applied magnetic field and can be manipulated by magnetic field gradients. Their magnetic susceptibility is several orders of magnitude larger than biological tissues [13], allowing the application of large forces. Biocompatible ferrofluids have been used to study mechanical properties inside living tissues *in vivo* [14, 15, 16, 17, 18] and functionalized nanoparticles have allowed targeting cellular components such as DNA and proteins with high specificity [19, 20] or to deliver drugs into compartments that are difficult to access as e.g., the inner ear [13].

Magnetic actuation offers several advantages over optical tweezers in the context of biological systems. First, biological tissues are fully transparent to magnetic fields. Forces can thus be exerted in a controlled way deep within the specimen regardless of its optical transparency. Second, magnetic fields do not induce heating, and, with the exception of magnetoreceptive species [21], most animals are insensitive to this physical parameter. Thus, besides the injection itself, this technique is physiologically non-invasive even for extremely large magnetic intensity.

Here we show that the injection of ferrofluid into the otic vesicle of larval zebrafish allows controlled magnetic forces to be exerted on the otolith, mimicking naturally occurring gravitational and acceleration forces. This fictive vestibular stimulation elicits strong and robust compensatory eye and tail movements, comparable to those evoked by roll or tilt motion of the animal over large angles. We simultaneously recorded the brain-wide neuronal activity evoked by this fictive vestibular stimulation using functional light-sheet microscopy. By

injecting the ferrofluid into a single ear we disentangled the contribution of each utricle to the brain-wide neuronal response, which is not possible under natural conditions when rotating the animal [4]. This constitutes the first use of a ferrofluid to stimulate a sensory system *in vivo*. The method is inexpensive, easy to implement and compatible with most neurophysiological recording methods such as large scale functional imaging, optogenetics or electrophysiology. This makes vestibular stimulation now as broadly accessible as visual stimulation and will allow researchers in various labs of different research focus to investigate the vestibular contribution to a large variety of behaviors and neuronal processes such as evidence accumulation, head direction circuits, decision making, cerebellar functions, motor learning and motor control and this in head attached or eventual even freely swimming assays.

2 Results

After ferrofluid injection into the otic vesicle, vestibular-driven behaviors can be evoked through magnetic stimulation

We injected a custom-made ferrofluid [22] into both inner ears of zebrafish larvae 5 days after fertilization (dpf). The ferrofluid consisted of 11 nm in diameter iron oxide (γ-Fe_2O_3) particles with citric acid surface functionalization to make them stable in water (pH 7, see Methods). After the injection, the otic vesicle maintained its shape and the ferrofluid was visible as a red-orange tinge (Figure 1A). The otolith itself, once dissected out and washed, also displayed a slight orange coloration, indicating that some of the injected ferrofluid particles had permanently bound to the otolith. The otolith was thus magnetized, as could be confirmed by approaching a permanent magnet to its proximity. The otolith immediately moved towards the magnet as shown in the Supplementary Figure S1.

Next, we tested whether this nanoparticle coating of the otolith could yield magnetic forces *in vivo* on the otolith comparable to the gravitational force that acts on it when the head/body is rolled or tilted in space (Figure 1B). To do so, we examined the behavioral response (compensatory eye and tail movements) that were induced through magnetic actuation. We thus immobilized a bilaterally injected fish in a drop of 2% low melting point agarose on a thin glass slide and removed the agarose around the eyes and tail to allow free movements (Figure 1C). The specimen was placed in a chamber filled with the embryonic medium E3. A front and a side camera were used to monitor the eyes and tail movements evoked by the in-plane movement of a small permanent neodymium magnet positioned beneath the fish.

We observed two distinct responses depending on the orientation of the movement with respect to the body axis. When the magnet was moved along the medio-lateral axis, the eyes rolled and the tail bent in a direction opposite to the magnet (Movie 4 Part I). Such movements are characteristic of responses elicited by a roll motion of the animal (i.e., a rotation along its longitudinal axis) via vestibulo-ocular and vestibulo-spinal reflexes [4, 8]. In this case, the magnetic force acted laterally on the otolith, as does the gravitational force during a roll motion. When the magnet was moved along the antero-posterior axis, the eyes rotated along the tilt axis and discrete swim bouts were triggered. Here the response to the magnetic stimulation was in line with compensatory eye movements and tail kinematics elicited upon tilting the fish [8] (see Movie 4 Part II).

To quantify these responses, we imposed controlled sinusoidal displacements to the magnet using a two-axis motorized stage either along the lateral axis (fictive roll stimulus) or along the antero-posterior axis (fictive tilt stimulus). We used a frequency of 0.5 Hz and an amplitude of 2.5 mm corresponding to the radius of the magnet (see the following section describing the numerical simulations for an estimation of the corresponding magnetic force). Typical behavioral responses of such recordings are shown in the Movie 4. We found the behavioral response to be strong in 80 % of the tested fish, which confirmed the robustness of the method. Importantly, the observed vestibular behaviors were reproducible and stable over time with only small variability over 150 stimulus repetitions in the same fish (Figure 1D). From the averaged cyclic ocular rotation signal, we extracted an angular range of $\alpha = 13.2^\circ \pm 7.4^\circ$ (mean ± standard deviation) during simulated roll motion and $\beta = 8^\circ \pm 4.3^\circ$ for simulated tilt motion (Figure 1). Interestingly, the behavioral responses were stronger for lower concentrations of injected ferrofluid (Figure 1E).

These values can be compared to those obtained during natural vestibular stimulation in which the animal is actually rolled or tilted in space. As an illustration, we show in Figure 1E the angular range ($\alpha = 14.1^\circ \pm 5.8^\circ$ (mean ± standard deviation) of eye rotation measured in larvae exposed to a sinusoidal roll motion of $\pm 15^\circ$. One may notice that both the mean and the standard deviation are comparable in both experiments, indicating that the large variability across specimen is not specific to the fictive ferromagnetic stimulation. From the roll motion-evoked responses, we calculated a gain of the roll vestibulo-ocular response in darkness of $g_{roll} = 0.5 \pm 0.2$ and for the ocular motor tilt response a gain of $g_{tilt} = 0.3$ is reported [8]. From this calibration, we thus estimated that the fictive magnetic vestibular roll and tilt stimuli corresponded to a peak-to-peak stimulus of $\alpha/g_{roll} \approx \pm 14^\circ \pm 27^\circ$ (mean ± std) and $\beta/g_{tilt} \approx \pm 7^\circ \pm 4^\circ$ (mean ± std), respectively.

Ferrofluid injection into the inner ear does nor impair vestibular function.

Hair cells in the vestibular system are sensitive to mechanical and chemical stress, which can lead to cell death, thus impairing sensory function [23]. We assessed possible damage induced by either the injection procedure or by the ferrofluid itself using a simple behavioral assay. Fish use their vestibular system to keep their dorsal side-up posture stable during swimming. Therefore, uncorrected rolling along the rostro-caudal body axis during a swim bout can be used as an indication of vestibular dysfunction [24, 25, 26] (Figure 2A). We quantified the outcome of this procedure by calculating a roll ratio, i.e., the proportion of roll events over a total of 5 swimming events after a mechanically evoked startle response [27] (see Methods). The roll ratio was measured at 2, 24 and 48 hours after the injection had been performed at 5 dpf.

Control (non-injected) fish had a mean roll ratio of 0.44 ± 0.36 (mean ± std, N = 10) at 5 dpf (Figure 2B). Although the vestibulo-ocular reflex is fully established at 5 dpf [8], vestibular-driven postural control is still being refined between 5 to 7 dpf as evidenced by the decrease of the roll ratio during this period. As a second (negative) control, we performed a similar assay on larvae injected bilaterally with the calcium chelator BAPTA (5 mM), which disassociates hair cell tip-links and disrupts the mechano-electrical transduction [28]. Two hours after the injection, the roll ratio was close to one (mean roll ratio: 0.93 ± 0.11, see Movie 4), indicative of an almost complete loss of vestibular-driven postural control. Tip links have been shown to regenerate in 8 to 24 hours [29]. Hence, 48 h after BAPTA injection, the roll ratio of the larvae were

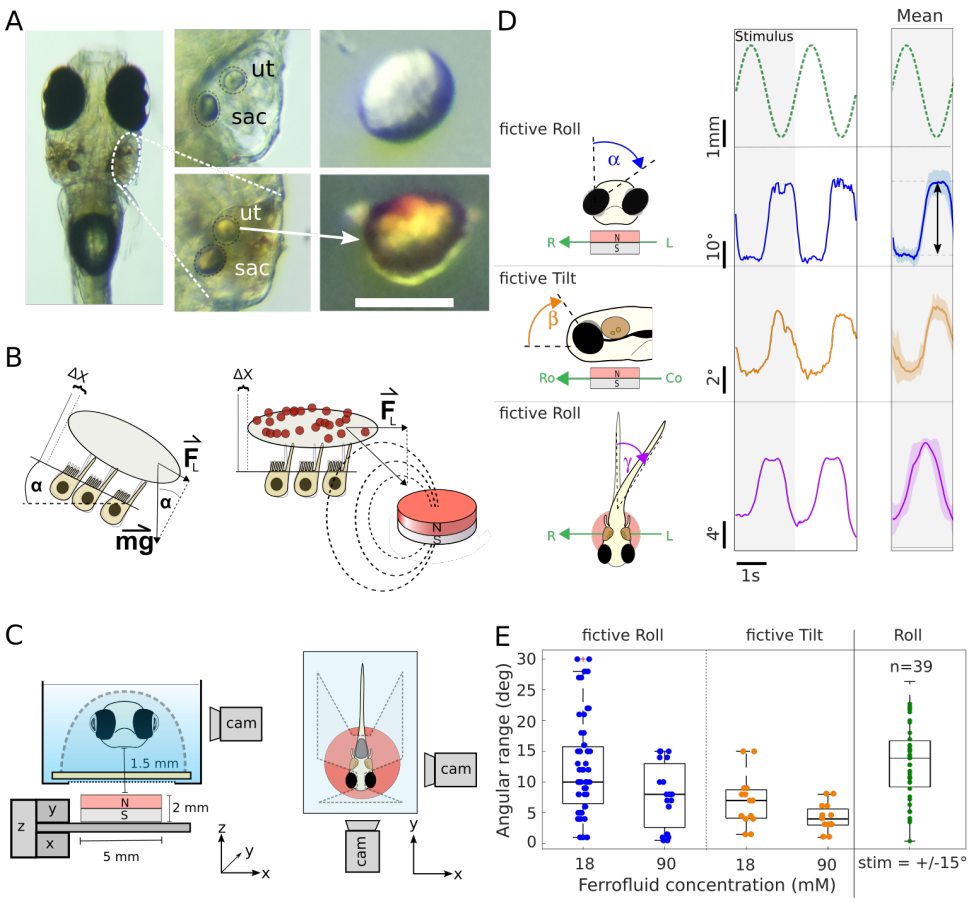

Figure 1: Magnetic actuation of the otoliths after surface coating by ferromagnetic nanoparticles. **A** Top view of a 5 dpf zebrafish larva after bilateral intra-otic ferrofluid injection. Middle column: Zoom onto the otic vesicle with injected ferrofluid (bottom) and before injection (top). The otoliths of the utricle, ut, and of the saccule, sac, are visible. Right: Bright-field image of an utricular otolith dissected from a control fish (top) and from a fish after ferrofluid injection (bottom). Attached iron nanoparticles appear in red-orange. Scale bar = 50 μm. **B** The diagram on the left illustrates the lateral force experienced by an otolith when the head is rotated relative to the gravitational field, $F_L = g \cdot sin(\alpha)$ (top). The right side illustrates an otolith covered with nanoparticles that exert a lateral force onto the otolith when placed in a magnetic field gradient. **C** Left: Diagram of the setup in front view. An x,y-motorized stage and a manual z-stage (black) move the magnet (red) under the head-tethered fish, mounted in agarose (outlined by a dashed line). Right: Top view of the setup illustrating the front and side cameras (cam) for eye motion tracking. The magnet center is aligned with the center of mass of the fish inner ears (not drawn to scale). **D** Evoked eye and tail movements in response to the magnet motion along different directions in a sinusoidal manner beneath a fish injected with 18 mM ferrofluid solution. Left column shows the two first cycles of a 150 repetition trial and right columns shows the average trial response and standard deviation. **E** Angular range of evoked eye rotation angles (peak-to-peak, see arrow in 1D) in response to fictive roll and tilt stimuli plotted for two concentrations of ferrofluid bilaterally injected into the inner ears ($N_{roll,18mM}$=24, $N_{roll,90mM}$=11, N_{tilt} = 9 for both concentrations).

significantly lowered and not significantly different anymore to control fish, reflecting a progressive recovery of posture control by tip link regeneration.

Next, we performed similar tests on buffer- and ferrofluid-injected fish, in order to disentangle the effect of the injection procedure from the ferrofluid itself on the vestibular system. Two hours after injection, the roll ratio (0.51 ± 0.31 and 0.65 ± 0.21, respectively) for both conditions were not significantly different from that of control fish (Tukey test $p > 0.1$). This remained so at 24 h and 48 h post injection. Finally, we injected DiASP that fluorescently labels functional hair cells as it diffuses through the mechanotransduction channels if mechanotransduction is functional. Hair cells became clearly labeled after the injection (see inset Figure 2B). Thus, neither the injection procedure itself nor the ferrofluid seem to significantly affect the function of the vestibular organs.

Finally, we examined the kinematics of free swimming behavior in ferrofluid-injected fish compared to uninjected control larvae. We found that inter-bout interval and turn angle distributions were not significantly different from control fish, while the average displacement per swim bout was only marginally increased (Figure S2 and Movie 4). The various tests confirmed that the ferrofluid injection procedure has a very limited impact on the functionality of the vestibular system and on the locomotor behavior.

Numerical simulations of the magnetic force exerted onto the magnetized otolith.

To evaluate the impact of magnetic forces on the nanoparticle-covered otolith and its dependency on the magnet position relative to the larva, we resorted to numerical simulations (Figure 3A). This approach revealed the existence of a range of magnet positions within which the force exerted onto the magnetized particle varies linearly with the radial distance to the center of the magnet. The force is maximal when the particle is located above the edge of the magnet beyond which it decreases and eventually vanishes. The maximal lateral force and the extent of the linear regime increases with magnet diameter, while the maximal force decayed as z^{-4} as expected for a magnetic dipole, where z is the vertical distance to the magnet. These results suggest that the magnet should be placed as close as possible beneath the fish and that horizontal displacements should remain smaller than the radius of the magnet. Under these conditions, the force-displacement relationship is expected to be linear.

To estimate the maximum force that can be imposed onto the otolith, we measured the velocity in water of an isolated otolith (obtained after dissection of an injected larva) submitted to a comparable magnetic field as in the *in vivo* experiment. Taking into account the otolith diameter, that controls the drag force, we obtained an estimated force of ~ 1 nN. We can then compare this value to the gravitational forces exerted on the otolith *in vivo* when the head is tilted in space. The utricular otolith in fish is a calcium carbonate (aragonite) crystal with a density of $2.83\,\mathrm{g.cm^{-3}}$ and a diameter of $\sim 55\,\mu m$ at the age of 6 dpf [9]. From these values, we estimated that under natural conditions, the maximal gravitational force experienced by the utricular otolith is ~ 1.6 nN when the fish is rolled 90°. The magnetic and gravitational forces acting on the otolith are thus in the same range, which *a posteriori* explains the capacity to drive large vestibular-like behavioral responses as detailed above.

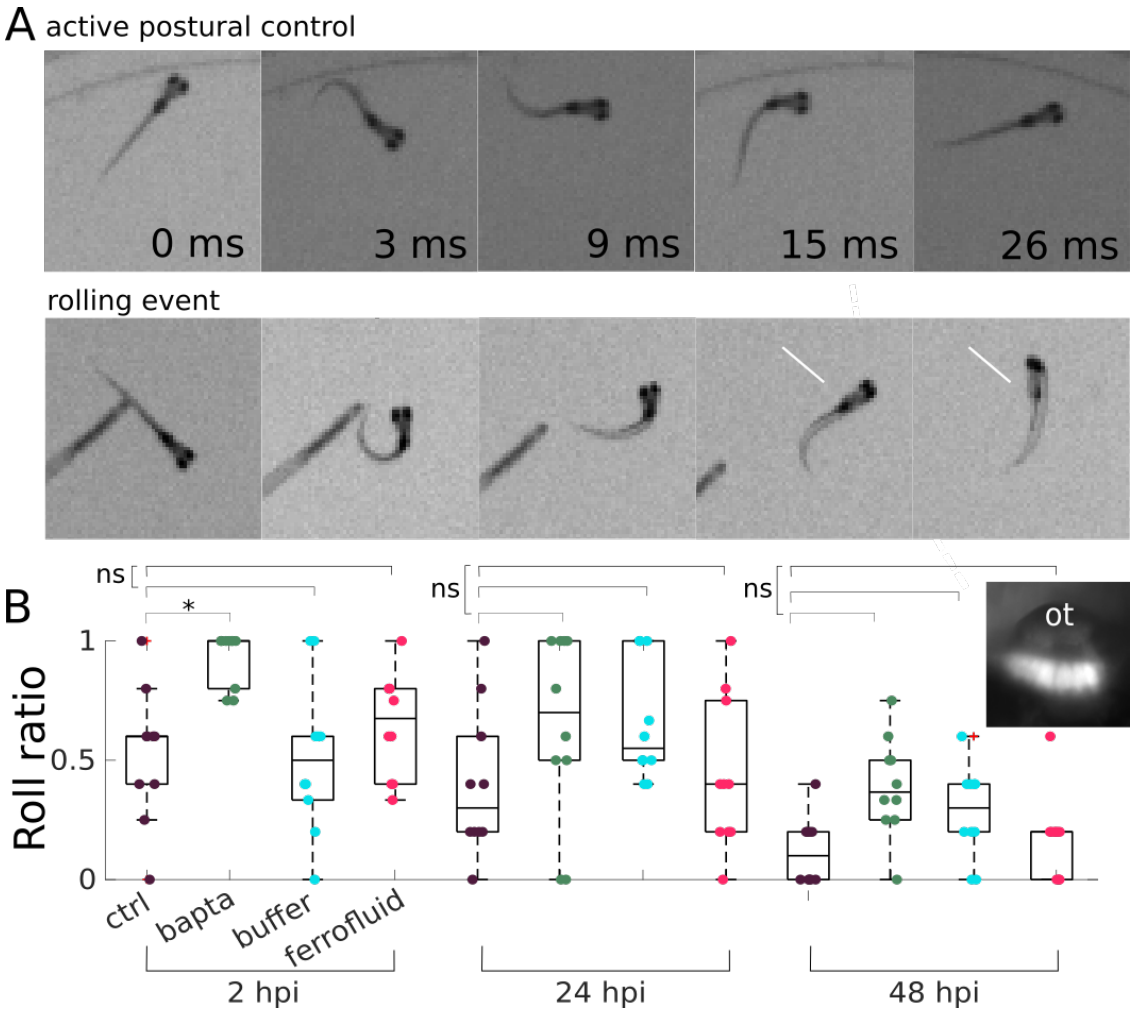

Figure 2: Control experiments probing the impact of the injection procedure on vestibular functionality **A** Image sequence recorded during evoked startle response behaviors for a non-injected control fish illustrating active postural control (top) as well as for BAPTA injected fish illustrating a roll event (bottom). **B** Roll ratio during an evoked startle response measured 2, 24 and 48 hours post bilateral injection (hpi) of BAPTA, ferrofluid or buffer compared to non-injected control fish from the same batch, respectively.

Our simulations can also be used to evaluate the number of nanoparticles attached to the otolith. A single particle experiences $\sim 0.007\,\mathrm{fN}$ of lateral force when placed at the edge of a 5 mm in diameter magnet positioned 2 mm beneath the particle. Therefore, approximately $1.4{\cdot}10^8$ particles are required to produce a total of 1 nN force. This corresponds to a ~ 1 monolayer of particles bound to the otolith. This fine coating represents only 0.2 ‰ of the mass of the otolith and is thus unlikely to interfere with the vestibular function, in agreement with our observations.

Brain-wide functional imaging during magnetic vestibular stimulation and behavioral monitoring

One of the assets of our stimulation technique is its low footprint, which facilitates a combination with

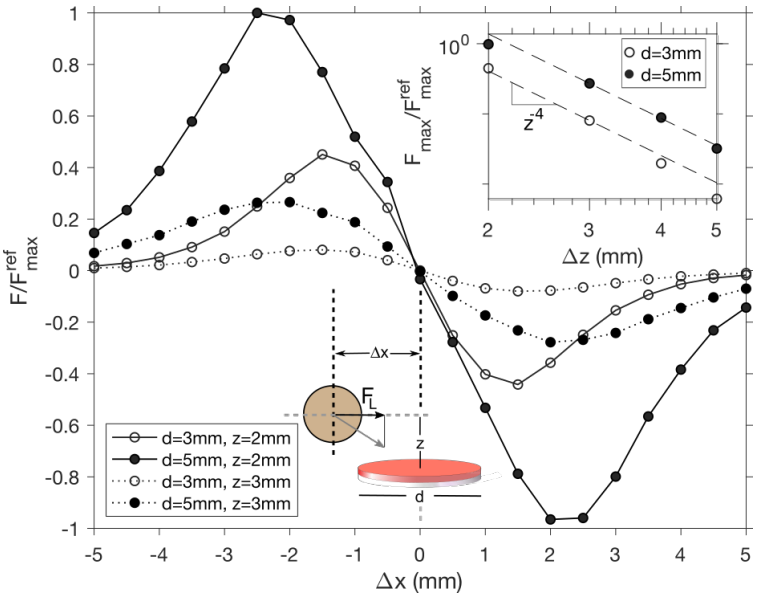

Figure 3: Simulations. Finite element simulation of the lateral force, F, exerted on a paramagnetic particle by a magnet as a function of the lateral distance (Δx) of the particle to the magnet's center axis. Shown are force-displacement relationships for two magnet diameters, d, and two z-distances, z, between the magnet and the particle. The calculated forces were normalized by the maximum of the force-displacement relation, F^{ref}_{max}, extracted from the configuration with the 5 mm in diameter magnet positioned at a distance of 2 mm. Inset: Dependency of the maximal lateral magnetic force, F_{max}, as function of the z-distance between the particle and the magnet, calculated for two magnet diameters.

any functional recording technique. Here we used a setup that enables the application of controlled fictive vestibular stimuli in head-tethered larval zebrafish while recording the behavioral responses as well as the evoked brain-wide neuronal activity using light-sheet imaging (Figure 4A).

We first recorded the neuronal activity, evoked in mechanosensitive inner ear hair cells. In order to do so, we used the transgenic line *α-tubulin:Gal4-VP16;UAS:GCaMP7*, which expresses the GCaMP7 calcium indicator in hair cells of the inner ear [30]. Both inner ears of these fish were injected with ferrofluid, embedded in agarose, and placed in the experimental setup one day after the injection. We generated a fictive vestibular roll stimulus by moving the magnet sinusoidally along the left-right body axis at 0.5 Hz and 2.5 mm amplitude. Hair cells in the anterior macula (AM, utricle) showed a modulation of the fluorescence signal, phase-coupled to the stimulus (Figure 4B). In contrast, hair cells in the posterior macula (PM), which are part of the saccule that senses vertical oscillations at higher (auditory) frequencies, showed no detectable response indicating that they were likely not stimulated. These observations are consistent with the anatomical orientation of the mechanosensitive axes of the two vestibular organs.

Next, we recorded the brain-wide neuronal dynamics elicited upon fictive vestibular stimulation using the pan-neuronal nuclear localized *Tg(elavl3:H2B-GCaMP6f)* transgenic line. This stimulus evoked neuronal activity throughout the brain (see Movie 5). As an example, we show activity time traces recorded from vestibulo-spinal neurons and from the oculomotor nucleus nIII (Figure 4C). We quantified the brain-wide

vestibular response pattern by computing a phase map as described in Migault *et al.* [4]. Briefly, we estimated, for each voxel (0.6x0.6x10μm), the amplitude and the phase relation of the evoked signal relative to the stimulus waveform. These two parameters were displayed in the form of a phase map, where color represents the relative phase of the neuronal response to the stimulus and intensity encodes the amplitude of the response. Hence, a phase shift of 0° applies to neurons whose activity is locked to the applied force, whereas a phase shift of 90° corresponds to neurons responding to the time-derivative of the force signal. Figure 4D shows the phase map for several selected layers and their z-projection, recorded in a single fish and registered on the Z-brain atlas [31]. Vestibular-induced activity is clearly visible in the tangential vestibular nucleus and in vestibulo-spinal neurons. The observed ocular motoneuron activity is consistent with the monitored compensatory eye movements. Active regions also include the nucleus of the medial longitudinal fascicle, as well as hindbrain pre-motor neuronal populations involved in tail motion. Cerebellar and inferior olivary neurons were also clearly recruited. This response map was found to be stereotypic and reproducible for all injected fish as shown by the sharpness of the average phase map, which combines the observations in 14 larvae (Figure 4E). This average phase map shows a close similarity with the brain-wide response recorded during natural vestibular stimulation using a rotating light-sheet microscope (Figure 4F and Figure 4 in Migault *et al.* [4].

This new stimulation method offers, as optical tweezers but in contrast to a natural stimulation, the opportunity to stimulate a single ear at a time, by injecting the ferrofluid only unilaterally. Figure 4G show the average phase map for fish injected with ferrofluid into the right ear only. Interestingly, the response appears rather similar to that evoked by bilateral fictive vestibular stimulation, albeit with a relatively lower intensity. The marked antisymmetric activity in the medial octovolateralis nucleus (MON) reflects a strong activity of commissural connections between both sides of the brain and suggests a pronounced contralateral inhibitory connectivity in the hindbrain.

We finally performed control experiments with non-injected fish. At the stimulation frequency, no signal was detectable in the average phase map (Figure 4H). This rules out the possibility that the recorded activity may in part reflect the visual stimulus caused by the moving magnet, which could have been possible as the blue (488 nm) laser forming the light sheet also illuminates the sample chamber.

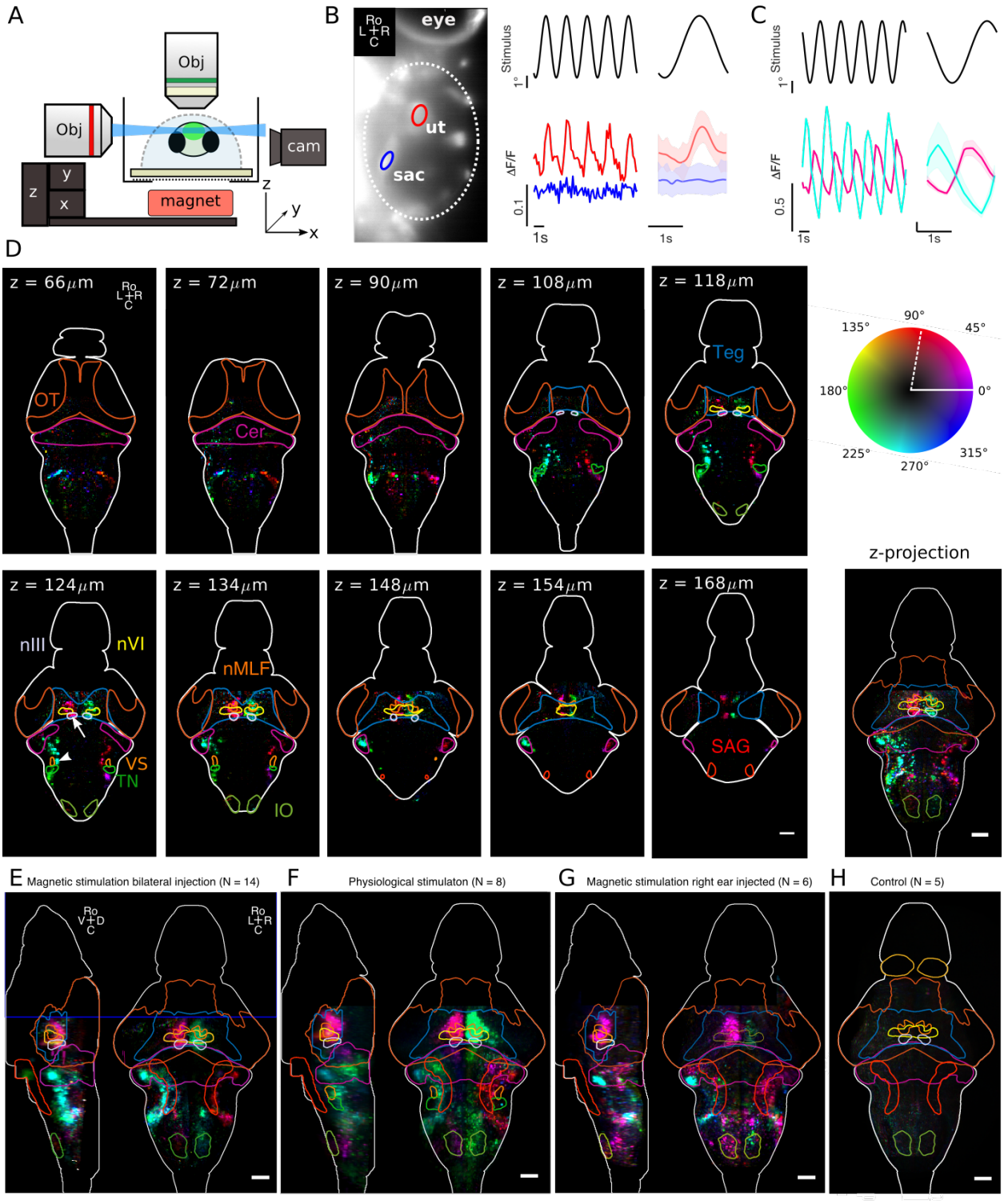

Figure 4: Brain-wide neuronal responses evoked by magnetic vestibular stimulation. Caption continues next page.

Figure 4: (Continued) **A** For functional imaging a light-sheet (blue) excites the fluorescence GCaMP6 sensor genetically encoded in the brain (green). The fluorescence is collected by an objective perpendicular to the light-sheet. **B** Calcium responses recorded in the otic vesicle from the utricle (red) and the saccule (blue) in response to a sinusoidal fictive roll stimulus (black). The trial-averaged response with std (N = 75 repetitions) is shown on the right. The ROIs from which the fluorescent signals were extracted are indicated with red and blue circles respectively. **C** Neuronal responses to the same stimulus as in **B** but measured in vestibulo-spinal neurons (white arrowhead in panel D) and extraocular motoneurons in the oculomotor nucleus (white arrow in panel **D** bottom left). **D** Selected layers of the phase map of the brain-wide response recorded in one fish. OT: optic tectum, Cer: cerebellum, Teg: tegmentum, nIII and nIV: oculomotor and trochlear nucleus, nMLF: nucleus of the medial longitudinal fascicle, SAG: statoacoustic ganglion, IO: inferior olive, TN: tangential nucleus, VS: vestibulo-spinal neurons. The color map indicates the phase of the neuronal response relative to the stimulus after correction for the phase delay introduced by the GCaMP6f calcium sensor $\Delta\phi = \arctan(-2\pi f \tau_{GCaMP6f})$(decay time $\tau_{GCaMP6f} \approx 1.8\,\mathrm{s}$). Without this correction the zero degree phase shift would be at the position indicated by the dashed white line. Bottom right: Maximum z-projection of the entire phase map shown of this fish. **E** Average phase map in response to bilateral fictive vestibular stimulation (N = 14 fish). **F** Average phase map recorded during natural vestibular stimulation with a rotating light-sheet microscope [4]. **G** Average phase map in response to unilateral (only right ear injected) fictive vestibular stimulation. **H** Control phase map recorded under the same conditions as **E and H** but without injected ferrofluid into the inner ear. Transgenic lines: *Tg(a-tubulin:Gal4-VP16 ;UAS:GCaMP7a)* panel B, *Tg(elavl3:H2B-GCaMP6f)* panel C-H.

3 Discussion

Our work demonstrates that injecting a ferrofluid solution into the inner ears of larval zebrafish allows to subsequently apply controlled forces to the utricular otolith *in vivo*, thus mimicking natural motion-like vestibular stimuli in immobilized animals. A small permanent magnet was sufficient to elicit robust motor responses to both fictive vestibular roll and tilt stimulation that were indistinguishable from those observed during natural motion stimulation. Cross-talk between the two stimulus directions was negligible, provided that the magnet was well centered beneath the fish.

Control experiments confirmed that the injection procedure did not damage the vestibular system and left the swimming behavior and postural control performance unaffected 24 hours after the injection. This robustness of the method reflects the minor interference of the injection procedure with the functionality of the system but may in part be related to the capacity of non-mammalian hair cells for self-repair [29]. Hence, even if tip-links were damaged by the injection procedure, the vestibular apparatus is likely fully functional 24 - 48 h post injection. In addition to potential tip-link repair, non-mammalian inner ear hair cells can regenerate destroyed hair cell bundles [32] and even full hair cells with restored sensory function after cell death [33, 34, 35]. In the adult zebrafish utricle, the full regeneration of the utricular macula after induced damage takes about 13 days [36]. This is too slow to explain the observed high performance of the vestibular system after injections leading to the conclusion that the injections did not cause substantial and functionally detrimental cell death.

Our proposed mechanism underpinning the fictive stimulation is based on the irreversible binding of nanoparticles onto the surface of the otolith. This thin magnetized coating can then be acted upon using magnetic field gradients. We reported direct evidence of the effective magnetization of the otolith and that the corresponding magnetic force is in the same order of magnitude as the gravitational force imposed during macroscopic body rotation. In the present study, we only tested two different concentrations of injected ferrofluid, and the strongest response was obtained already at the lowest concentration. This observation suggests that a relatively small number of nanoparticles is sufficient to entirely cover the otolith with a compact monolayer. Any further particles are then likely to be repelled from the surface due to electrostatic repulsion between the citric acid-coated nanoparticles.

A complementary mechanism may be at play that would rely on the magnet-induced motion of freely floating nanoparticles in the endolymphatic otic environment. The induced fluid motion would then impose a drag force onto the otolith. Given the nano-bead dimensions, the associated flow would be in the low Reynolds number regime and the particles are thus expected to reach their terminal velocity in less than a millisecond when placed in a field gradient. The resulting drag force, proportional to this particle velocity, would vary with the magnet position and could not be distinguished from the direct magnetic actuation on the otolith. However, an estimate of the particle terminal velocity results in a value of $\approx 0.1\,\mu m/s$, which in turn yields a drag force orders of magnitude smaller than the force exerted by the particles attached to the otolith. This suggests that this second mechanism is probably negligible.

In zebrafish, the utricular otolith is spherical. For a spherical mass, the gravitational force grows with the radius cubed while the magnetic force acting on a thin surface coating grows with the radius squared. One may thus anticipate that this magnetic actuation method should become relatively inefficient for larger animals (with larger otoliths). However, in most animals other than teleost fish, the otolithic membrane is covered with small carbon crystals called otoconia yielding a flat meshwork of extended mass. This leads to a much higher surface to volume ratio, which is more favorable for the actuation via surface-bound nanoparticles. Our method could thus work also in larger animals such as for instance *Xenopus* larvae, lampreys or even mammalian species provided that sufficiently strong magnetic fields and field gradients can be delivered. In fact, a pilot study on an isolated *in vitro* preparation of *Xenopus* tadpoles at mid-larval stage, demonstrated that solutions of citrate-coated ferromagnetic nanoparticles can be reliably injected and distributed throughout the duct system of the inner ear. Repetitive displacement of a permanent point magnet above the transparent otic capsule in different directions, elicited faithful and robust eye movements also in these animals (see Movie 4), which are an order of magnitude larger than larval zebrafish. The known functionality of all inner ear organs at this developmental stage ([37]), however, renders an identification of the recruited vestibular organ(s) more difficult but potentially derives from the magnetic stimulation of multiple inner ear organs.

This magnetic actuation method was implemented to fictively stimulate a slow tilt or roll of the fish body. However, the same approach could be used to mimic translational accelerations experienced by the larvae during free swimming. Larval zebrafish swimming patterns consist of discrete swim bouts that last for $100 - 200\,\text{ms}$ interspersed by $\sim 1\,\text{s}$-long resting periods. Owing to the Einstein principle, otoliths are

actuated during these transient linear accelerations: forward acceleration of the animal produces a backwards pointing force on the otolith while a deceleration corresponds to a forward pointing force. The reported peak acceleration during a bout is in the range of $0.3 - 2\,\mathrm{m/s^2} = 0.03 - 0.2\,\mathrm{g}$ [38, 39], which corresponds to a force on the otolith in the range of $50 - 300\,\mathrm{pN}$, i.e., within the accessible range of our instrument. To mimic acceleration forces encountered during a swim bout, the magnet has to be moved by $0.3 - 2\,\mathrm{mm}$ in about $50\,\mathrm{ms}$, which is also compatible with the performance of our mechanical stages. Our system can thus be used to emulate vestibular signals associated with fictive self motion in head-fixed animals. It could thus be included into closed-loop virtual reality assays, mitigating sensory mismatch and enhancing the quality of virtual environments. This will open new possibilities to study sensorimotor processing.

Unlike other approaches, such as optical tweezers, the reported method could potentially be implemented in freely swimming configurations as well. A large scale magnetic field gradient could be used to create a sufficiently large force onto the magnetized otolith coating to counteract the gravitational force acting on it. One could thus create a zero gravity condition or mimic inverted gravity and study how fish adapt to and learn to cope with this change of physical parameters. As only injected fish will be sensitive to the applied magnetic field gradients, social behavior experiments can be envisioned to study how conspecific fish react to behavioral changes of a single fish when the latter experiences a perturbation of the vestibular sensation. But one may even go beyond and investigate how animals can learn to use this novel sensation of magnetic field gradients, e.g. for navigational strategies.

We have demonstrated that our vestibular stimulation method is compatible with simultaneous whole-brain functional imaging using light-sheet microscopy. In response to the fictive vestibular stimulus, we observed consistent neuronal activity in the vestibular nucleus and in downstream nuclei throughout the brain. The evoked neuronal response map in bilaterally injected fish was comparable to the one that was obtained during actual vestibular motion stimulation with a rotating light-sheet microscope. This confirms that the magnetic force acts without delay onto the otolith in the same manner as gravitational forces when the animal is e.g., rolled along its longitudinal body axis. The recorded average phase maps during unilateral stimulation suggests the presence of a pronounced commissural inhibition between the two vestibular nuclei, typically conserved in all vertebrates [40]. Sinusoidal magnetic stimulation of the right ear shows that pulling the right otolith laterally activates neurons located in the right vestibular nucleus and downstream regions such as the ipsilateral vestibular cerebellum, and on the contralateral side oculomotor motoneurons, neurons in the nMLF as well as hindbrain neuronal populations probably projecting to the spinal chord. This activity pattern and profile is consistent with the highly conserved axonal projections from the vestibular nucleus to these brain regions [41, 42]. This activation pattern has a mirror-symmetric counterpart with a mean activity that is 180 degrees phase-shifted and thus exhibits a mean activity that is minimal when the mirror-symmetric neuronal correlate is maximally active. This suggests that the vestibular nucleus inhibits the contralateral vestibular nucleus, which leads to a reduced activity in downstream nuclei. The latter result is consistent with the description of inhibitory commissural projections in cats between vestibular neurons of the utricular pathway [43], which are thought to contribute to the sensitivity of vestibular neurons through a disinhibition [43]. In larval zebrafish, commissural projections have been described as originating from the tangential vestibular nucleus [8], with a likely inhibitory function as evidenced by our results.

In summary, our magnet-based vestibular stimulation method is inexpensive, easy to implement, and can be developed as an add-on device for existing microscopes and visual virtual reality setups. Since the magnet is small and operates beneath the fish, the whole experimental chamber is accessible for all types of microscopes, optogenetic tools, electrophysiological setups, other sensory stimulation methods or behavioral monitoring. Accordingly, our method uniquely expands the toolbox of widely accessible sensory stimulation methods for zebrafish systems neuroscience but also for neuroscientific studies in other species.

4 Movie legends

Movie 1

Behavioral responses to fictive magnetic vestibular stimulation with a hand-held magnet.
Part I: Behavioral response to fictive vestibular roll stimulation recorded by top view monitoring. The fish is tethered with the agarose that was removed around the tail and eyes to allow free movements. The movie was obtained with a stereomicroscope immediately after ferrofluid injection. The magnet was hand-held and moved beneath the fish along the left-right body axis to mimic a vestibular roll stimulus.
Part II: Same fish as in Part I, with the magnet moved along the rostro-caudal body axis to mimic a tilt stimulus (nose-up, nose-down).
Eyes and tail perform marked compensatory movements in response to these fictive vestibular stimuli.

Movie 2

Behavioral responses to fictive vestibular roll and tilt stimuli generated and recorded in an automatized setup. Ferrofluid was bilaterally injected at 5 dpf and movies were recorded the next day at 6 dpf. The magnet was moved sinusoidally at 0.5 Hz and with 2.5 mm amplitude. **Part I:** Front view of evoked eye movements in response to a fictive roll stimulus.
Part II: Side view of evoked eye movements in response to a fictive roll stimulus. The eye rotates only along the roll axis and not along the tilt axis, demonstrating the absence of cross-talk between the two stimulation axes.
Part III: Side view of evoked eye movements in response to a fictive tilt stimulus. **Part IV:** Top view of evoked tail movements in response to a fictive roll stimulus. Note that the magnet created a shadow under the fish, which allows to see the correlation between magnet displacement and tail movement.

Movie 3

Impaired postural control along the roll axis after BAPTA injection compared to wild-type control fish with an intact vestibular system.
Part I: The movie shows a fish two hours after bilateral injection of the calcium chelator BAPTA. The fish was placed freely in a Petri dish filled with embryonic medium E3 and recorded from the top. A startle response was elicited by touching the fish with a fine glass tip. During the startle response and also during successive swimming bouts, the fish lost its dorsal position and rolled around its longitudinal body axis.

Part II: Recording of a wild-type control fish under the same conditions as in Part I. Throughout the sequence and including the startle response, the fish maintained its dorsal side-up posture.

Movie 4

Free swimming behavior of fish, injected bilaterally with ferrofluid, compared to wild-type control fish (Recording frame rate = 70 fps):
Part I: Wild-type fish (N = 10) swimming freely in a Petri dish.
Part II: Fish after bilateral injection of ferrofluid into the inner ears (N = 7), swimming freely in a Petri dish.

Movie 5

Brain-wide neuronal responses during a fictive sinusoidal roll stimulus.
The movie shows in a loop the neuronal response averaged over 40 stimulus cycles. Six sections of the brain are shown.
Experimental parameters: Ferrofluid was injected bilaterally at 5 dpf into a fish of the Tg(elav3-H2B:GCaMP6f) transgenic line. The movie was recorded the next day at 6 dpf. The magnet was moved sinusoidally at a frequency of 0.5 Hz and with an amplitude of 2.5 mm.

The phase map in Figure 4D was calculated from this recording.

Movie 6

Pilot study in a *Xenopus* tadpole.
The movie shows a dorsal view of an isolated *in vitro* preparation of a *Xenopus* tadpole prepared following the protocol in Lambert *et al.* 2008 [37]. Ferrofluid was injected into the left inner ear (red-orange color). A permanent point magnet was displaced in close proximity above the inner ear. The magnet motion provoked eye rotations via the vestibulo-ocular reflex. Only the left eye responded as the right eye was partly immobilized to hold the preparation in place.

STAR METHODS

KEY RESOURCES TABLE

REAGENT OR RESOURCES	SOURCE	IDENTIFIER
Chemicals		
Low melting point agarose	Sigma-Aldrich	A9414-50G
Tricaine	Sigma-Aldrich	E10521-10G
Ferrofluid	custom made	[22]
BAPTA	Sigma-Aldrich	14510-100MG-F
2-Di-4-Asp	Sigma-Aldrich	D3418-500MG
Ultrapure Low Melting Point Agarose	Invitrogen	16520050
Experimental Models: Organisms/Strains		
Tg(a-tubulin:Gal4-VP16 ;UAS:GCaMP7a)		Köster and Fraser 2001 [30]
Tg(elav3-H2B:GCaMP6f)		Vladimirov et al. 2014 [44]
Software and Algorithms		
Matlab	The MathWorks	https://www.mathworks.com/products.html
CMTK	Rohlfing and Maurer, 2003 (citation)	https://www.nitrc.org/projects/cmtk/
FIJI	(ImageJ) NIH	https://fiji.sc/
ZBrain atlas	Randlett et al., 2015	https://zebrafishexplorer.zib.de/home/
Comsol Multiphysics	Comsol	https://www.comsol.com/
Other		
Pneumatic PicoPump	World Precision Instruments	SYS-PV830
Glass capillaries to pull micropipettes	Warner Instruments	GC100F-10
Micropipette puller	Narishige	PC-100
Motorized stages	Physik Instrumente PI	PIMag® Linear Stage: V-408.132020, V-408.232020
Behavior tracking: Camera	Point Grey	BFLY-U3-05S2M-CS
Behavior tracking: Objective	Navitar	1-61449
Behavior tracking: 2x Adaptor	Navitar	1-61450
Magnet (D=5 mm, thickness 1 mm, 3 magnets stacked)	RS Components	N837RS
Micro knife 22,5° cutting angle	Fine Science Tools	10316-14

Table 1: Key resource table

EXPERIMENTAL MODEL AND SUBJECT DETAILS

Animal husbandry

All experiments were performed on 5-7 dpf larvae. Adult fish were maintained at 28°C in system water (ph 7-7.5 and conductivity between 300 and 350 μS)) in the fish facility of the Institut de Biologie Paris-Seine. Eggs were collected in the morning and then kept in a Petri dish with E3 at 28°C in a 14h/10h light/dark cycle. Larvae were fed with paramecia or powder from 5 dpf on. Calcium imaging experiments were carried out in two different transgenic lines: *elavl3:H2B-GCaMP6f* [44] (kindly provided by Misha Arhens) and *α-tubulin:Gal4-VP16 ;UAS:GCaMP7* [30] (kindly provided by Teresa Nicolson) both in Nacre background. Experiments were approved by Le Comité d'Éthique pour l'Expérimentation Animale Charles Darwin C2EA-05 (02601.01 and 32423-202107121527185 v3).

METHOD DETAILS

Ferrofluid

The ferrofluid, a suspension of γ-Fe_2O_3 iron oxide nanoparticles, was produced by Christine Ménager and Aude Michel Tourgis (Sorbonne Université, Laboratoire PHENIX, CNRS UMR 8234) following the protocol described by Massart et al. [22] and kindly provided to us for our experiments. The hydrodynamic diameter measured by dynamic light scattering (DLS) was 22 nm with a polydispersity index of 0.15. This corresponds to a physical diameter of 11 nm, usually measured by TEM after drying the sample. The particles were dispersed in water and stabilized with citrate molecules at pH 7 to prevent agglomeration.

Ear injections

Either ferrofluid, BAPTA or 4-Di-1-ASP were injected into the inner ear with a glass micropipette held by a micromanipulator (Narishige MN-153) using a pneumatic Pico-pump (World Precision Instruments PV830). Capillaries (1 mm outer diameter, Warner Instruments GC100F-10) were pulled to obtain fine tip micropipettes (tip diameter = 1 - 2 μm) using a Narishige PC-100 puller with the following parameters: 2 steps, Heater N°1 = 52,4; Heater N°2 = 55,7, position 2 mm, 2 heavy and 1 light weights. Micropipettes were loaded with 2 μL of ferrofluid diluted in buffer (NaCl 0.178 M, sodium citrate 0.023 M, HEPES 0.01 M) at 0,019 μM. Injections were performed in 5 dpf fish. Larvae were mounted dorsal side up in 2 % LMP agarose on top of a microscope glass slide. Using a small piece of metal as support, the slide was rolled 45 degrees to access the fish's left ear. For the ferrofluid, 3 pulses (10 psi for 500 ms) were injected into the otic vesicle, corresponding to a total volume of 1,2 nL. After the left ear injection, the glass slide was rolled onto the other side to inject the right ear. For injection of BAPTA and DiASP the protocol was the same except for different concentrations of the solutions. We used 50 mM BAPTA dissolved in extracellular solution containing (in mM) 134 NaCl, 2.9 KCl, 1.2 $MgCl_2$, 2.1 $CaCl_2$, 10 HEPES, and 10 glucose, at 290 mOsm, adjusted to a pH 7.8 with NaOH. For 4-Di-1-ASP, a 50 mM solution of diluted E3 medium containing 1% ethanol was injected. After the injections, larvae were freed from the agarose using a fine tip (Dumont n°5) and maintained in E3 medium until the experiments commenced.

Roll ratio essay

The larvae were placed in a 5 cm Petri dish positioned under a high magnification objective and recorded at 300 fps. Approaching the larvae with a fin glass tip evoked a startle response. Each larva was subjected to five trials. The roll behavior was assessed for each trial. The roll ratio was calculated as the number of trials the animal rolled during an escape divided by the number of trials the animal attempted an escape [27].

Sample preparation

24 hours after ferrofluid injection larvae were mounted in 2 % low melting point agarose dorsal side-up on top of a small acrylic holder (1mm thick). Then, the holder was placed inside an acrylic chamber filled with E3. For behavioral experiments, the agarose was removed from the eyes and tail using a micro knife (FST Micro Knife - Plastic Handle/22.5° Cutting Angle).

The setup

We built a platform with two motorized stages (PI instruments) to precisely control the magnet position and hence the fictive vestibular stimulation. A third manual stage allowed to position the magnet beneath the fish as close as possible in the vertical plane in order to maximize the accessible range of force. For the experiments shown in Figure 1 and 4 we used a magnet 5 mm in diameter and 3 mm in height. Injected fish were mounted in a drop of 2% low melting point agarose on top of a transparent acrylic holder (1 mm thick). The agarose was removed from around the eyes and tail to allow unimpaired movements. Then, the holder was placed into the sample chamber filled with embryonic medium E3. The bottom of the sample chamber was formed by a 220μm thick coverslip glass. A front and a side camera were installed to record eye movements. To record tail movements, we used the same camera as for the neural recordings, equipped with a 4x objective. The entire platform was mounted on a light-sheet microscope system to perform simultaneous brain-wide neuronal activity recordings.

Behavioral protocol

In order to move the magnet in a controlled manner, we used 2 stages for x and y axis movements (Physik Instrumente, V-408 PIMag Linear Stage). To simulate a roll-like motion, we moved the magnet along the transverse axis, starting from the center and extending 2.5 mm towards each side of the fish. To simulate a tilt-like motion, we moved the magnet along the longitudinal axis, using the same amplitude. The stimulation frequency was 0.5 Hz.

Imaging Setup

The imaging setup was built around a microscope frame (Scientifica Slicescope Pro) fitted with an Olympus BX-URA fluorescence illuminator and a custom light-sheet forming unit adapted from Migault et al. [4]. Functional imaging was performed with a Leica HC FLUOTAR L 25x/0,95 W VISIR objective and a Hamamatsu Orca-Flash4.0 V3. Images were recorded with HCImage software (Hamamatsu) and the light-sheet was controlled with a custom application written in Matlab (MathWorks). Top view behavioral recordings used the microscope's light path and camera with a Nikon CFI Achro 4x objective. Side and front view behavioral recordings used separate systems of Point Grey cameras (BFLY-U3-05S2M-CS) with Navitar Precise Eye objectives (1-61450 with 1-61449).

QUANTIFICATION AND STATISTICAL ANALYSIS

Free swimming control

We analyzed the free swimming behavior of ferrofluid-injected and control fish. Seven larvae were injected at 5 dpf. 24 hours later they were placed in a Petri dish to record the swimming behavior during 1 hour at 30 fps. The movies were tracked using FastTrack [45]. Individual fish were not tracked throughout the whole movie but rather split into wall-to-wall trajectories. For each trajectory, discrete swim bouts were detected when the instantaneous swim speed exceeded two times the overall variance of the speed. Putative bouts were then filtered on a distance criterion: bouts with a linear displacement – measured in a time window of

±0.5 s centered on the bout velocity peak – less than 0.3 mm or greater than 18 mm were rejected) and on a temporal criterion (bouts occurring within 0.4 s after a bout were rejected. Bout onset was defined at 80 ms before the velocity peak. From positions, time and body angles before and after an event, the inter-bout interval, displacement and turn angles associated with each bout were computed. These values were then averaged over trajectories and the means were displayed as boxplots. Mean square displacement (MSD) was computed using the MATLAB package msdanalyzer [46]. (x,y) sequences were pooled by condition (control and injected), a MSD was computed for each sequence and the ensemble average is presented along with the standard error of the mean.

Finite element simulations and force generation mechanism

Force of a ferrofluid particle in a magnetic field gradient The ferrofluid particles are so small that nanoparticles consist only of a single magnetic domain giving the particle a giant magnetic moment. In the absence of an external magnetic field, the direction of this moment changes randomly depending on the temperature. The average magnetisation is zero and the particle is in a superparamagnetic state. In an external magnetic field, the giant magnetic moment becomes progressively aligned against the thermal agitation, and the average net magnetization increases. The macroscopic magnetization of a ferrofluid particle or of a ferrofluid droplet is characterized by the macroscopic magnetic moment, $\vec{m}$, which depends on the volume V of the particle or of a ferrofluid droplet, and the external field B. In a weak magnetic field the macroscopic magnetization is given by

$$\vec{m}(\vec{B}) = \frac{V\chi}{\mu_0}\vec{B}$$

with χ the magnetic susceptibility and μ_0 the vacuum permeability. And the force exerted on the droplet reads

$$\vec{F} = \nabla\left(\vec{m}(\vec{B})\cdot\vec{B}\right) = \nabla\left(\frac{V\chi}{\mu_0}\vec{B}^2\right) = 2\frac{V\chi}{\mu_0}\vec{B}\nabla\vec{B}$$

In a strong field that saturates the magnetization the force exerted on the droplet is

$$\vec{F} = \nabla\left(\vec{m}_{sat}\cdot\vec{B}\right) = \vec{m}_{sat}\nabla\vec{B}$$

Finite element simulations We used Comsol Multiphysics to calculate the magnetic force applied by the magnet to the ferrofluid. Lateral force-displacement curves were calculated for cylindrical magnets of different diameters and z-distance to a spherical droplet of the ferrofluid with a diameter of 200 μm. The spherical droplet was considered perfectly rigid. The droplet volume was chosen arbitrarily. The force, acting on the droplet depends linearly on the volume of the droplet. Therefore uncertainty with respect to the droplet volume will change the maximum force reached but not the linear dependence of force on the magnet position. The relationship between magnetic flux density and magnetic field strength (B-H curve) is defined for the ferrofluid by a magnetization curve (Figure S3). The magnetic flux density is fixed for the magnets.

For the simulations, we started with a mesh size of 500 μm and then iteratively reduced the mesh size until the results converged. Parametric sweeps were realized for different distances and diameters.

The simulation gives a maximal lateral force of $F_{D=200\,\mu} = 4 \cdot 10^{-4} N$ exerted on the ferrofluid droplet with a diameter of $D = 200\,\mu m$ placed 2 mm above our 5 mm in diameter magnet. As the force depends linearly on the volume we estimated that the force exerted on a single nanoparticle with a diameter of $D = 11\,nm$ is $F_p = 0.007\,\mathrm{fN}$.

Drag force on an otolith pulled through water To estimate the maximum force that can be delivered to the otolith, we measured the velocity in water of an isolated otolith (obtained after dissection of an injected larvae) submitted to a comparable magnetic field as in the *in vivo* experiment. Taking into account the otolith diameter that controls the drag force, we obtained an estimated force of

$$F_{drag} = 6\pi\eta R v = 0.9\,\mathrm{nN}$$

with η the viscosity of water $R = 27.5\,\mu$m, the radius of the otolith and v the speed at which the otolith was dragged by the magnet through the aqueous solution.

Given the force that the magnet exerts on a single particle of the ferrofluid suspension $F_p = 0.007\,\mathrm{fN}$ we can estimate the number of particle bound to the otolith

$$N = \frac{F_{drag}}{F_p} = 1.3 \cdot 10^8$$

A monolayer of particles on the otolith surface corresponds to

$$N \approx \frac{4\pi R_{otolith}^2}{D_p} = 0.8 \cdot 10^8$$

particles. Thus we estimate that ~ 1.6 monolayers of particles have bound to the otolith.

However, due to the small diameter of the particles, the mass change of the otolith is negligible with

$$\frac{m_{monolayer}}{m_{otolith}} = \frac{4\pi R_{otolith}^2 D_p \cdot \rho_{Fe_2O_3}}{4/3\pi R_{otolith}^3} = 2 \cdot 10^{-4}$$

Gravitational force F_g exerted onto the otolith during roll motion When the fish is rolled under natural conditions along the rostro-caudal body axis, gravity acts on the otoliths pulling them along the left-right body axis. The magnitude of this lateral component of the gravitational force F_g depends on the roll angle and on the density of the otolith

$$F_g = (\rho_o - \rho_w) V_o g \sin(\alpha)$$

with the density of the otolith $\rho_o = 2.83\,\mathrm{g\,cm^{-3}}$, the density of water $\rho_o = 1\,\mathrm{g\,cm^{-3}}$, the otolith volume $V_o = \frac{4}{3}\pi R_o^3$, the otolith radius $R_o = 27\,\mathrm{nm}$, the gravitational acceleration $g = 9.81\,\mathrm{m\,s^{-2}}$ and the angle α by which the animal is rolled relative to its dorsal side-up position.

At $\alpha = 90°$ the lateral force on the otolith is maximal with:

$$F_g(\alpha = 90°) = 1.6\,nN$$

Because the mean behavioral response in the fictive roll motion experiments compares to the mean evoked response when rolling fish with a sinusoidally modulated excursion of ±15°, we can estimate that we exerted *in vivo* with our experimental parameters in average a force of $< F_{max} >= 1.6\,\mathrm{nN} \cdot \sin(15°) = 400\,\mathrm{pN}$ on the otolith when displacing the magnet $2.5\,mm$.

Time constant at which a particle reaches its terminal velocity when accelerated by a constant force in a viscous solution. Freely floating particles in the inner ear will be accelerated by the magnet. However, due to the interaction with the surrounding water molecules they will reach a terminal velocity after a characteristic time

$$\tau = \frac{m_p}{6\pi\eta R_p} = \frac{2\rho_p R_p^2}{9\eta} = 516\,\mathrm{ps}$$

with the particle mass m_p, the hydrodynamic particle radius $R_p = 22\,nm$ and the viscosity of water η. The terminal velocity reached is

$$v = \frac{F}{6\pi\eta R_p} = 0.1\,\mu\mathrm{m\,s}{-1}$$

with the hydrodynamic particle radius $R_p = 22\,nm$ and the viscosity of water η and with the estimated maximal force $F_p = 0.007\,\mathrm{fN}$ exerted on a ferrofluid nanoparticle placed 2 mm over the edge of our 5 mm in diameter magnet.

Calcium imaging analysis and phase map calculation

Image pre-processing and calcium transient (ΔF/F) extraction were performed offline using MATLAB, according to the workflow previously reported [4].

Registration onto the Z-Brain atlas

We used the Computational Morphometry ToolKit CMTK (http://www.nitrc.org/projects/cmtk/) to compute for every fish the morphing transformation from the average brain stack (anatomical stack) to the Elavl3:H2B-RFP stack of the zBrain atlas [31]. This allowed mapping the functional data onto the Z-Brain Viewer, to overlay the region outlines and to calculate averages across animals.

We computed first the affine transformation, which we used then as initialization to compute the warp transformation between the two stacks. The used commands and options are listed in table 2.

Tool	Options	Description
cmtk registration	–Initxlate –dofs 6,9,12 –sampling 3 –coarsest 25 –omit-original-data –accuracy 3 –exploration 25.6	Calculate affine transformation
cmtk warp	-v -–fast –grid-spacing 40 –refine 2 –jacobian-weight 0.001 –coarsest 6.4 –sampling 3.2 –accuracy 3.2 –omit-original-data	Use affine transformation as initialization
reformatx		Apply transformation to other stacks

Table 2: CMTK commands and options

RESOURCE AVAILABILITY

Lead contact

Further information and requests for resources and reagents should be directed to and will be fulfilled by the lead contact, Volker Bormuth (volker.bormuth@upmc.fr).

Data and code availability

Data reported in this and any additional information required to reanalyze the data is available from the lead contact upon request.

Acknowledgements

We thank Christine Ménager and Aude Michel Tourgis (Sorbonne Université, Laboratoire PHENIX, CNRS UMR 8234) who kindly provided the ferrofluid. We thank the IBPS fish facility staff for the fish maintenance, in particular Stéphane Tronche and Alex Bois. We thank Misha Ahrens and Teresa Nicolson for providing transgenic fish lines. We are grateful to Carounagarane Dore for his contribution to the design of the experimental setup. We thank Claire Wyart and Marcus Ghosh for their comments on the manuscript. This project has received funding from the European Research Council (ERC) under the European Union's Horizon 2020 research innovation program grant agreement number 715980, and was partially funded by

the CNRS, Sorbonne Université, and by the German Science Foundation through the collaborative research center 870 (CRC 870). H.M., G.M., and P.T. had a PhD fellowship from the Doctoral School in Physics, Ile de France (EDPIF). G.L.G. had a PhD fellowship from the Systems Biology Network of Sorbonne Université.

Authors contribution

N.B., H.S., N.D, G.D. and V.B designed the project. N.B., H.M., G.M. and P.T. performed the zebrafish experiments. N.B. T.Panier, T. Pujol, G.M, and V.B. built the experimental setup. T.Pujol performed the finite element simulations. N.B., H.M., G.M., G.L.G., P.T., G.D., V.B. analyzed the data, N.D. and H.S. performed the *Xenopus* experiment. N.B., G.D., V.B wrote the manuscript with input from all the authors.

Declaration of interests

The authors declare no competing interests.

References

1. Angelaki DE and Cullen KE. Vestibular system: the many facets of a multimodal sense. English. Annual review of neuroscience 2008; 31:125–50. DOI: 10.1146/annurev.neuro.31.060407.125555
2. Cullen KE. The vestibular system: Multimodal integration and encoding of self-motion for motor control. Trends in Neurosciences 2012; 35:185–96. DOI: 10.1016/j.tins.2011.12.001. Available from: http://dx.doi.org/10.1016/j.tins.2011.12.001
3. Panier T, Romano SA, Olive R, Pietri T, Sumbre G, Candelier R, and Debrégeas G. Fast functional imaging of multiple brain regions in intact zebrafish larvae using Selective Plane Illumination Microscopy. English. Frontiers in neural circuits 2013; 7:65. DOI: 10.3389/fncir.2013.00065
4. Migault G, Plas TL van der, Trentesaux H, Panier T, Candelier R, Proville R, Englitz B, Debrégeas G, and Bormuth V. Whole-Brain Calcium Imaging during Physiological Vestibular Stimulation in Larval Zebrafish. Current Biology 2018. DOI: 10.1016/j.cub.2018.10.017
5. Favre-Bulle IA, Vanwalleghem G, Taylor MA, Rubinsztein-Dunlop H, and Scott EK. Cellular-Resolution Imaging of Vestibular Processing across the Larval Zebrafish Brain. Current Biology 2018 Dec; 28:3711–3722.e3. DOI: 10.1016/j.cub.2018.09.060
6. Ahrens MB, Orger MB, Robson DN, Li JM, and Keller PJ. Whole-brain functional imaging at cellular resolution using light-sheet microscopy. English. Nature methods 2013; 10:413–20. DOI: 10.1038/nmeth.2434
7. Beck JC, Gilland E, Tank DW, and Baker R. Quantifying the ontogeny of optokinetic and vestibuloocular behaviors in zebrafish, medaka, and goldfish. Journal of Neurophysiology 2004 Dec; 92:3546–61. DOI: 10.1152/jn.00311.2004. Available from: https://www.physiology.org/doi/10.1152/jn.00311.2004

8. Bianco IH, Ma LH, Schoppik D, Robson DN, Orger MB, Beck JC, Li JM, Schier AF, Engert F, and Baker R. The tangential nucleus controls a gravito-inertial vestibulo-ocular reflex. Current Biology 2012; 22:1285–95. DOI: 10.1016/j.cub.2012.05.026

9. Favre-Bulle IA, Stilgoe AB, Rubinsztein-Dunlop H, and Scott EK. Optical trapping of otoliths drives vestibular behaviours in larval zebrafish. Nature Communications 2017; 8. DOI: 10.1038/s41467-017-00713-2. Available from: http://dx.doi.org/10.1038/s41467-017-00713-2

10. Mo W, Chen F, Nechiporuk A, and Nicolson T. Quantification of vestibular-induced eye movements in zebrafish larvae. BMC neuroscience 2010; 11:110. DOI: 10.1186/1471-2202-11-110

11. Ehrlich DE and Schoppik D. Control of Movement Initiation Underlies the Development of Balance. Current Biology 2017 Feb; 27:334–44. DOI: 10.1016/j.cub.2016.12.003

12. Voit W, Kim DK, Zapka W, Muhammed M, and Rao KV. Magnetic behavior of coated superparamagnetic iron oxide nanoparticles in ferrofluids. MRS Online Proceedings Library 2011; 676:78. DOI: 10.1557/PROC-676-Y7.8. Available from: https://doi.org/10.1557/PROC-676-Y7.8

13. Shapiro B, Kulkarni S, Nacev A, Sarwar A, Preciado D, and Depireux D. Shaping Magnetic Fields to Direct Therapy to Ears and Eyes. Annual Review of Biomedical Engineering 2014; 16:455–81. DOI: 10.1146/annurev-bioeng-071813-105206

14. Desprat N, Supatto W, Pouille PA, Beaurepaire E, and Farge E. Tissue Deformation Modulates Twist Expression to Determine Anterior Midgut Differentiation in Drosophila Embryos. Developmental Cell 2008; 15:470–7. DOI: 10.1016/j.devcel.2008.07.009

15. Doubrovinski K, Swan M, Polyakov O, and Wieschaus EF. Measurement of cortical elasticity in Drosophila melanogaster embryos using ferrofluids. Proceedings of the National Academy of Sciences of the United States of America 2017 Jan; 114:1051–6. DOI: 10.1073/PNAS.1616659114

16. Fernández-Sánchez ME, Barbier S, Whitehead J, Béalle G, Michel A, Latorre-Ossa H, Rey C, Fouassier L, Claperon A, Brullé L, Girard E, Servant N, Rio-Frio T, Marie H, Lesieur S, Housset C, Gennisson JL, Tanter M, Ménager C, Fre S, Robine S, and Farge E. Mechanical induction of the tumorigenic β-catenin pathway by tumour growth pressure. Nature 2015; 523:92–5. DOI: 10.1038/nature14329. Available from: https://doi.org/10.1038/nature14329

17. Mitrossilis D, Röper JC, Le Roy D, Driquez B, Michel A, Ménager C, Shaw G, Le Denmat S, Ranno L, Dumas-Bouchiat F, Dempsey NM, and Farge E. Mechanotransductive cascade of Myo-II-dependent mesoderm and endoderm invaginations in embryo gastrulation. Nature Communications 2017; 8:13883. DOI: 10.1038/ncomms13883. Available from: https://doi.org/10.1038/ncomms13883

18. Serwane F, Mongera A, Rowghanian P, Kealhofer DA, Lucio AA, Hockenbery ZM, and Campàs O. In vivo quantification of spatially varying mechanical properties in developing tissues. Nature Methods 2017; 14:181–6. DOI: 10.1038/nmeth.4101. Available from: https://doi.org/10.1038/nmeth.4101

19. Strick TR, Allemand JF, Bensimon D, Bensimon A, and Croquette V. The Elasticity of a Single Supercoiled DNA Molecule. Science 1996; 271:1835–7. DOI: 10.1126/science.271.5257.1835. eprint: https://science.sciencemag.org/content/271/5257/1835.full.pdf. Available from: https://science.sciencemag.org/content/271/5257/1835

20. Adhikari AS, Chai J, and Dunn AR. Mechanical Load Induces a 100-Fold Increase in the Rate of Collagen Proteolysis by MMP-1. Journal of the American Chemical Society 2011 Feb; 133:1686–9. DOI: 10.1021/ja109972p. Available from: https://doi.org/10.1021/ja109972p

21. Nimpf S, Nordmann GC, Kagerbauer D, Malkemper EP, Landler L, Papadaki-Anastasopoulou A, Ushakova L, Wenninger-Weinzierl A, Novatchkova M, Vincent P, Lendl T, Colombini M, Mason MJ, and Keays DA. A Putative Mechanism for Magnetoreception by Electromagnetic Induction in the Pigeon Inner Ear. Current Biology 2019; 29:4052–4059.e4. DOI: 10.1016/j.cub.2019.09.048

22. Massart R, Dubois E, Cabuil V, and Hasmonay E. Preparation and properties of monodisperse magnetic fluids. Journal of Magnetism and Magnetic Materials 1995; 149:1–5. DOI: 10.1016/0304-8853(95)00316-9

23. Schuknecht HF and Montandon P. Pathology of the ear in pneumococcal meningitis. Archiv für klinische und experimentelle Ohren-, Nasen-und Kehlkopfheilkunde 1970; 195:207–25

24. Riley BB and Moorman SJ. Development of utricular otoliths, but not saccular otoliths, is necessary for vestibular function and survival in zebrafish. Journal of Neurobiology 2000 Jun; 43:329–37. DOI: 10.1002/1097-4695(20000615)43:4<329::AID-NEU2>3.0.CO;2-H

25. Bagnall MW and McLean DL. Modular organization of axial microcircuits in zebrafish. Science 2014; 343:197–200. DOI: 10.1126/science.1245629

26. Roberts R, Elsner J, and Bagnall MW. Delayed Otolith Development Does Not Impair Vestibular Circuit Formation in Zebrafish. JARO - Journal of the Association for Research in Otolaryngology 2017; 18:415–25. DOI: 10.1007/s10162-017-0617-9

27. Hubbard JM, Böhm UL, Prendergast A, Tseng PEB, Newman M, Stokes C, and Wyart C. Intraspinal Sensory Neurons Provide Powerful Inhibition to Motor Circuits Ensuring Postural Control during Locomotion. Current Biology 2016; 26:2841–53. DOI: 10.1016/j.cub.2016.08.026

28. Assad JA, Shepherd GM, and Corey DP. Tip-link integrity and mechanical transduction in vertebrate hair cells. Neuron 1991; 7:985–94. DOI: 10.1016/0896-6273(91)90343-X

29. Zhao YD, Yamoah EN, and Gillespie PG. Regeneration of broken tip links and restoration of mechanical transduction in hair cells. Proceedings of the National Academy of Sciences of the United States of America 1996 Dec; 93:15469–74. DOI: 10.1073/pnas.93.26.15469. Available from: /pmc/articles/PMC26428/%20/pmc/articles/PMC26428/?report=abstract%20https://www.ncbi.nlm.nih.gov/pmc/articles/PMC26428/

30. Köster RW and Fraser SE. Tracing transgene expression in living zebrafish embryos. Developmental Biology 2001 May; 233:329–46. DOI: 10.1006/dbio.2001.0242

31. Randlett O, Wee CL, Naumann EA, Nnaemeka O, Schoppik D, Fitzgerald JE, Portugues R, Lacoste AMB, Riegler C, Engert F, and Schier AF. Whole-brain activity mapping onto a zebrafish brain atlas. Nature methods 2015; 12:1039–46. DOI: 10.1038/nmeth.3581

32. Harris Ja, Cheng AG, Cunningham LL, MacDonald G, Raible DW, and Rubel EW. Neomycin-induced hair cell death and rapid regeneration in the lateral line of zebrafish (Danio rerio). Journal of the Association for Research in Otolaryngology : JARO 2003 Jun; 4:219–34. DOI: 10.1007/s10162-

002-3022-x. Available from: http://www.pubmedcentral.nih.gov/articlerender.fcgi?artid=3202713&tool=pmcentrez&rendertype=abstract

33. Cotanche DA. Regeneration of hair cell stereociliary bundles in the chick cochlea following severe acoustic trauma. Hearing research 1987; 30:181–95

34. Girod DA, Duckert LG, and Rubel EW. Possible precursors of regenerated hair cells in the avian cochlea following acoustic trauma. Hearing research 1989; 42:175–94

35. Jones JE and Corwin JT. Regeneration of sensory cells after laser ablation in the lateral line system: hair cell lineage and macrophage behavior revealed by time-lapse video microscopy. eng. The Journal of neuroscience : the official journal of the Society for Neuroscience 1996 Jan; 16:649–62. DOI: 10.1523/JNEUROSCI.16-02-00649.1996

36. Jimenez E, Slevin CC, Colón-Cruz L, and Burgess SM. Vestibular and Auditory Hair Cell Regeneration Following Targeted Ablation of Hair Cells With Diphtheria Toxin in Zebrafish. Frontiers in Cellular Neuroscience 2021; 15:721950. DOI: 10.3389/fncel.2021.721950

37. Lambert FM, Beck JC, Baker R, and Straka H. Semicircular Canal Size Determines the Developmental Onset of Angular Vestibuloocular Reflexes in Larval Xenopus. Journal of Neuroscience 2008; 28:8086–95. DOI: 10.1523/jneurosci.1288-08.2008

38. Ehrlich DE and Schoppik D. A primal role for the vestibular sense in the development of coordinated locomotion. eLife 2019 Oct; 8. DOI: 10.7554/eLife.45839

39. Pozo Ad, Manuel R, Gonzalez ABI, Koning HK, Habicher J, Zhang H, Allalou A, Kullander K, and Boije H. Behavioral Characterization of dmrt3a Mutant Zebrafish Reveals Crucial Aspects of Vertebrate Locomotion through Phenotypes Related to Acceleration. eNeuro 2020; 7:ENEURO.0047–20.2020. DOI: 10.1523/eneuro.0047-20.2020

40. Malinvaud D, Vassias I, Reichenberger I, Rossert C, and Straka H. Functional Organization of Vestibular Commissural Connections in Frog. Journal of Neuroscience 2010; 30:3310–25. DOI: 10.1523/jneurosci.5318-09.2010

41. Highstein SM, Goldberg JM, Moschovakis AK, and Fernandez C. Inputs from regularly and irregularly discharging vestibular nerve afferents to secondary neurons in the vestibular nuclei of the squirrel monkey. II. Correlation with output pathways of secondary neurons. Journal of Neurophysiology 1987; 58:719–38. DOI: 10.1152/jn.1987.58.4.719

42. Straka H and Baker R. Vestibular blueprint in early vertebrates. Frontiers in Neural Circuits 2013; 7:1–9. DOI: 10.3389/fncir.2013.00182. Available from: http://journal.frontiersin.org/article/10.3389/fncir.2013.00182/abstract

43. Uchino Y, Sato H, Zakir M, Kushiro K, Imagawa M, Ogawa Y, Ono S, Meng H, Zhang X, Katsuta M, Isu N, and Wilson VJ. Commissural effects in the otolith system. Experimental Brain Research 2001; 137:421–30. DOI: 10.1007/s002210000611

44. Vladimirov N, Mu Y, Kawashima T, Bennett DV, Yang CT, Looger LL, Keller PJ, Freeman J, and Ahrens MB. Light-sheet functional imaging in fictively behaving zebrafish. English. Nature methods 2014; 11:883–4. DOI: 10.1038/nmeth.3040

45. Gallois B and Candelier R. FastTrack: An open-source software for tracking varying numbers of deformable objects. PLoS Computational Biology 2021; 17:e1008697. DOI: 10.1371/journal.pcbi.1008697. eprint: 2011.06837

46. Tarantino N, Tinevez JY, Crowell EF, Boisson B, Henriques R, Mhlanga M, Agou F, Israël A, and Laplantine E. TNF and IL-1 exhibit distinct ubiquitin requirements for inducing NEMO–IKK supramolecular structures. The Journal of Cell Biology 2014; 204:231–45. DOI: 10.1083/jcb.201307172

Supplementary Information

Supplementary figures

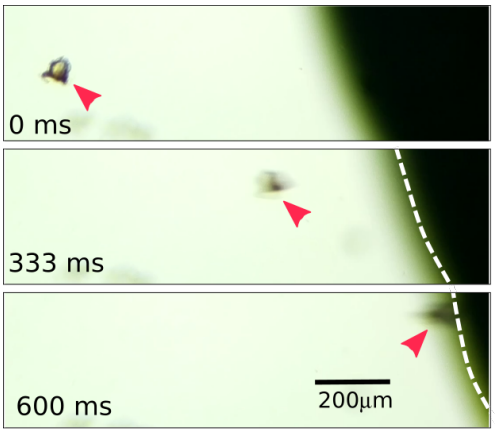

Figure S1: Image sequence of the dissected otolith (red arrowheads) with attached magnetic nanoparticles being attracted by a magnet (d = 5 mm) over time (dashed line indicates the magnet's edge) Related to Figure 1.

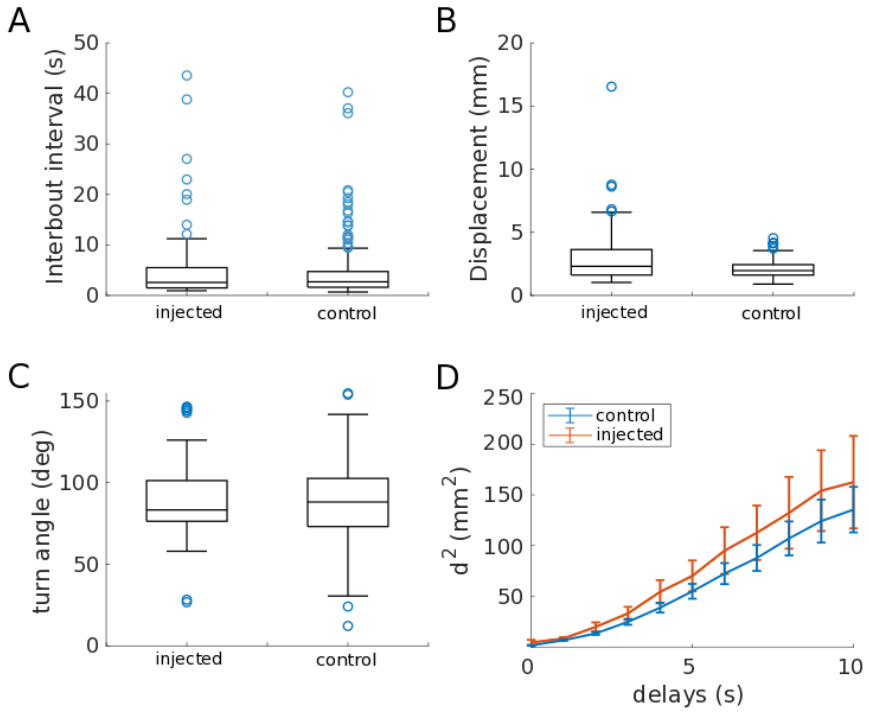

Figure S2: Effect of ferrofluid injection on swimming behavior. **(A-C)** Boxplots showing: **(A)** the distribution of the inter-bout interval, which is the time in seconds elapsed between two consecutive swimming events, **(B)** the mean displacement after a swim bout in mm, and **(C)** the turn angle in degrees. **(D)** Plot showing the mean of the mean square distance for 10 different time delay. The results were obtained by tracking two different batches of injected and non-injected fish. The fish were filmed swimming freely during 1 h (75 fps). P-values : ib-interval p = 0.846, displacement p = 0.00077, turn angle p = 0.366. N = 6 injected fish, 11 control non-injected fish. Related to Figure 1.

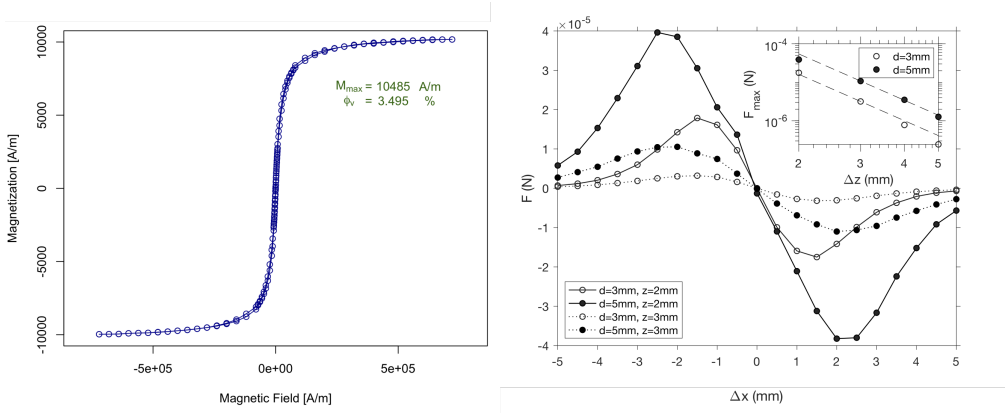

Figure S3: Left: Magnetization of the ferrofluid as a function of the magnetic field intensity (H). In vacuum, magnetic field intensity and magnetic flux density are linked by $\vec{B} = \mu_0 \vec{H}$. Right: Non-normalized simulation results. Related to Figure 3.